

# Hydrodynamically Modulated Alternating Current Voltammetry

Sheila A. Schuette<sup>1</sup> and Richard L. McCreery\*

Department of Chemistry, The Ohio State University, Columbus, Ohio 43210

**A new method for analytical voltammetry based on potential and hydrodynamic modulation is described. A 25  $\mu\text{m}$  diameter Pt wire vibrated perpendicular to its axis at a frequency of  $f_h$  exhibits a hydrodynamically modulated current at frequency  $2f_h$ . This alternating current (ac) is selective for mass transport controlled processes and insensitive to many background processes common to solid electrodes. When a low-frequency ( $<10$  Hz) potential modulation at frequency  $f_E$  is simultaneously imposed on the vibrating microwire, the hydrodynamically modulated current is amplitude modulated, resulting in ac components at  $2f_h \pm f_E$ . These components may be monitored to produce ac voltammograms with very low background currents. Low background response leads to improved detection limits and an extended anodic range for platinum electrodes in water. A semiempirical theory is developed which predicts the form of the double modulated current, based on simple hydrodynamic approximations. The experimental results are consistent with theoretical predictions, as demonstrated by the appearance of raw current waveforms, their Fourier transforms, and the ac voltammograms recorded at various demodulation frequencies. Detection limits in the submicromolar range are demonstrated for a ferrocene derivative monitored in aqueous solution with a Pt microwire electrode.**

Voltammetric methods of analysis have been developed extensively since their origin with dc polarography in the 1920s, with much of the driving force being the inherently high sensitivity of amperometric techniques. A large number of variants on classical voltammetry have been created, involving different potential waveforms, forced convection, numerous electrode shapes, and a variety of signal processing approaches. These methods share several common motivations. First, they seek to improve analytical detection limits by either increasing the signal or decreasing the capacitive background current, or both. Second, several methods have been developed to reduce the Faradaic background current resulting from surface or solvent reactions, which can be a major source of interference, particularly on solid electrodes. Third, resolution is enhanced by derivative or differential methods, where a peak shaped voltammogram is obtained rather than the waves common to dc polarography. Fourth, information about redox potential and reaction mechanisms can be obtained on a time scale from microsecond to D.C.

Despite this large research effort spanning several decades, voltammetry at low concentrations using solid electrodes remains a difficult venture. The background processes on platinum or carbon electrodes can be much larger than the Faradaic current for a dissolved analyte, even at analyte concentrations of ca.  $1 \times 10^{-5}$  M. The presence of these interfering processes greatly complicates solid electrode voltammetry at the nanomolar levels possible with mercury electrodes and precludes the use of the wider potential range available with carbon and platinum electrodes. This problem

is often severe for aqueous solutions, which make up the bulk of likely analytical samples. The desire to extend the useful potential range for trace voltammetry to more positive potentials than is possible with mercury electrodes has stimulated research on methods which reduce the Faradaic background current on solid electrodes, particularly in the positive potential regions where the use of mercury is precluded by its oxidation. A promising approach is hydrodynamic modulation voltammetry (HMV) in which the hydrodynamic mass transport rate to a solid electrode is varied periodically (1). Since surface Faradaic processes such as oxide formation are not mass transport controlled, their magnitudes will not vary with time. Since only the modulated current is monitored, large ( $\sim 100\times$ ) improvements in background rejection may be obtained, and solution components may be monitored more selectively. Several hydrodynamic modulation approaches have been pursued, including sinusoidal variation of rotation speed of a rotating disk electrode (RDE) (2-6), pulsed variation of RDE speed (7), pulsed flow in tubular electrodes (8-15), and HMV on vibrating wire (16, 17) and microwire (18) electrodes. As pointed out earlier (18), these HMV methods have good background rejection and sensitivity, with detection limits in the  $10^{-9}$ - $10^{-7}$  M range.

The technique to be described here is a previously unreported combination of hydrodynamic modulation voltammetry (HMV) and ac voltammetry with the objective of improving trace voltammetry on solid electrodes. As will be demonstrated below, the new method combines the excellent background rejection characteristics of HMV with the resolution of ac voltammetry, to yield trace voltammograms on solid electrodes in water at  $10^{-7}$  M levels, as well as extending the usable anodic potential range. The approach involves a double modulation experiment where both the hydrodynamic mass transport rate and the applied potential are varied simultaneously. The resulting alternating current contains components of both the hydrodynamic and potential modulation fundamental frequencies, in addition to the sum and difference frequencies produced by the two fundamentals. We will show that the sum frequency can be monitored as a function of potential to produce a peak-shaped voltammogram with excellent background rejection. Alternatively, the output can be considered to be an amplitude modulated sine wave at the hydrodynamic fundamental frequency. This double modulation approach retains the positive features of both HMV and ac voltammetry but allows measurements which are not possible with either method alone. The double modulated technique will be referred to as hydrodynamically modulated alternating current voltammetry (HMACV).

## THEORY

The hydrodynamic modulation method to be used was reported earlier (18) and exploits the properties of microwire electrodes which are vibrated perpendicular to their axis. This configuration permits higher modulation frequencies and lower sample volumes than are possible with an RDE, tubular, or conventional wire electrodes, but has the consequence of less well defined hydrodynamics. This fact necessitates a semiempirical formulation of the hydrodynamic current. Given this empirical relationship between current and electrode vibration velocity, a modulated potential may be incorporated

<sup>1</sup> Present address: Monsanto Co., St. Louis, MO 63198.

to produce a complex current waveform which includes both potential and hydrodynamic modulation. This waveform may then be analyzed for particular frequencies to demonstrate the analytical potential of the approach.

The raw current for HMAVCV may be predicted by using an approximate theory based on the Nernst diffusion layer model. Consider the general equation for Faradaic current for a reduction (eq 1), based on the generalized mass transport

$$\frac{i}{nFA} = m_0(C_{ox}^b - C_{ox}^s) \quad (1)$$

parameter  $m_0$  (19).  $C_{ox}^b$  and  $C_{ox}^s$  are the bulk and surface concentrations, respectively, for the reactant of the Faradaic process. For the steady-state condition in a convective system,  $m_0$  is a constant dependent on the particular convective arrangement and has been determined analytically for certain well-behaved systems like the RDE. For the case of a microwire electrode vibrating perpendicular to its axis, it has been demonstrated empirically that the current and, therefore,  $m_0$  are monotonic functions of the scalar electrode velocity through the solution (18). A wire electrode vibrating normal to its axis has been used for voltammetry for 3 decades (20, 21) and has been discussed recently in more sophisticated form (22, 23). These previous experiments were directed toward producing a steady-state current similar to that obtained at the RDE, and no consideration was given to hydrodynamic modulation. The approach described here has two distinctive features compared to these steady-state methods. First, the amplitude of vibration (ca. 1 mm) is much larger than the wire diameter (25  $\mu\text{m}$ ). Second, we are interested in the *modulated* (i.e. ac) hydrodynamic current, not merely the increase in steady-state current from vibration. For our case, as for that of Pratt and Johnson (16, 17), we are interested in the variations in current with electrode velocity, which in turn yield the hydrodynamically modulated ac response. Since the modulation amplitude is large relative to the electrode diameter, the wire is being swept through the solution at a varying velocity and, to a first approximation, will behave like a stationary electrode with fluid moving past at some scalar velocity,  $U$ . For this situation, it has been shown (24–26) that  $m_0$  will be proportional to  $U$  raised to some power  $x$ , where  $x$  is in the range 0.25–1. For an electrode oscillating at frequency  $f_h$ , the position and electrode scalar velocity of the electrode relative to the solution are given by eq 2 and 3, respectively, where  $K$  and  $K'$  are constants (the latter of which will include a function of the diffusion coefficient) and  $t$  is time. For both hydrodynamic and potential modulation

$$\text{position} = K \sin(2\pi f_h t) \quad (2)$$

$$U = \text{scalar velocity} = K' |2\pi f_h \cos(2\pi f_h t)| \quad (3)$$

$$m_0 = K'' |f_h \cos(2\pi f_h t)|^x \quad (4)$$

effects, the phase terms in sinusoidal expressions are ignored for the sake of simplicity. In real systems, the current does not decrease to zero when the electrode speed equals zero, and the modulation depth is not generally 100%. The mass transport parameter  $m_0$  is thus more accurately represented by

$$m_0 = m_{ss} + M m_{ss} |\cos(2\pi f_h t)|^x \quad (5)$$

where  $M$  is the modulation depth relative to the steady-state response and  $m_{ss}$  is the steady-state dc mass transport coefficient. As defined here,  $M$  includes  $K'$  and  $f_h^x$  and it has a frequency and geometry-dependent value between 0 and 1 for 25–100  $\mu\text{m}$  electrode diameters (18). Because of the absolute value function in eq 5,  $M$  will equal the ratio of the peak to peak amplitude of the current waveform to the magnitude to

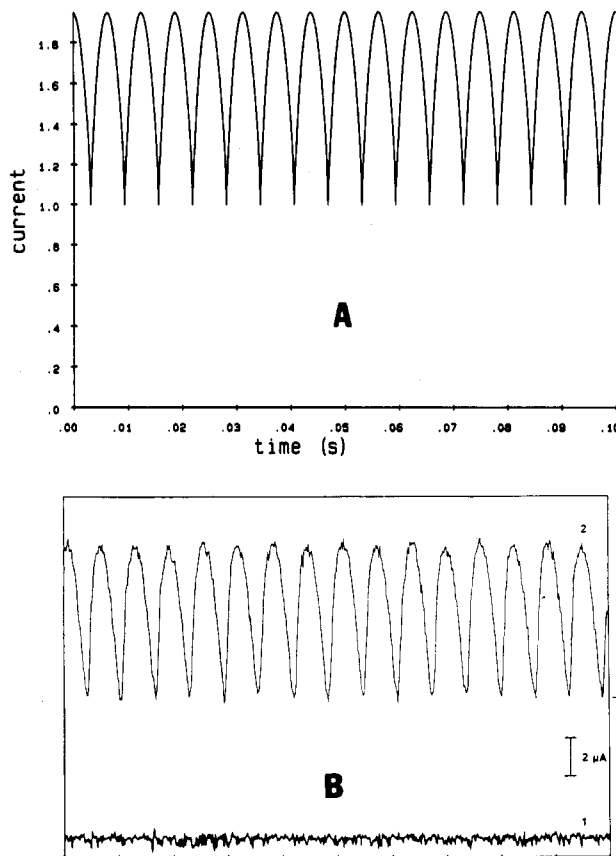


**Figure 1.** Mass transport limited raw current from a 25- $\mu\text{m}$  Pt wire for 0.91 mM ferrocene in 0.1 M TBAP/acetonitrile: (A) theoretical current calculated from eq 6 for  $f_h = 80$  Hz,  $M = 0.95$ ,  $x = 0.7$ ,  $E_{dc} = E^\circ + 150$  mV, current scale equals  $1/nFAC^\circ m_{ss}$ ; (B) experimental results for  $f_h = 80$  Hz,  $E = E^\circ + 150$  mV (curve 2) or  $E_{DC} = 0.00$  V vs. SCE (curve 1). Figure 1B appeared originally in ref 18.

the current at its minimum value.

At a mass transport limited potential, the current waveform will have the shape predicted by eq 1 and 5, with  $C_{ox}^s = 0$ . By fitting the experimental data to eq 5,  $x$  was found to be 0.7, and eq 6 was found to be a reasonable approximation of

$$i_h = nF A m_{ss} + nF A M m_{ss} |\cos 2\pi f_h t|^{0.7} \quad (6)$$

the hydrodynamic current, despite the complexity of the hydrodynamic situation. The ac current calculated from eq 6 is shown in Figure 1A for a diffusion-limited potential. Its appearance is that of a full wave rectified function of the electrode velocity and can be considered a distorted sine wave with fundamental frequency  $2f_h$ .

For steady-state mass transport with no hydrodynamic modulation, the potential dependence of the current for a reversible system is easily calculated by assuming that the surface concentration of the oxidized species is driven by the applied potential via the Nernst equation. If the potential is modulated, the resulting current waveform is similar to that obtained with ac polarography (27), except that the mass transport is at a convective steady state rather than solely diffusion controlled. The current for steady-state mass transport is given by

$$i_E = nF A M_0 C^b \left( \frac{1}{1 + \theta} \right) \quad (7)$$

where

$$\theta = \exp \left[ \frac{nF}{RT} \left( E_{dc} - E^\circ + \frac{\Delta E_{pp}}{2} \sin(2\pi f_E t) \right) \right]$$

Consider a vibrated microwire electrode whose current is governed by eq 1 and 5. If the potential is varied slowly relative to  $f_h$ , the current will vary predictably as  $C_{ox}^0$  is altered by the applied potential. In the limit of small  $f_E$ , one is merely scanning the potential sinusoidally and the result is a hydrodynamically modulated current whose magnitude tracks the applied potential. The situation can be described mathematically by substituting eq 5 in eq 7, to produce eq 8. The

$$i_{total} = nFAC_{ox}^0 \left( \frac{1}{1 + \theta} \right) [m_{ss} + m_{ss}M] \cos(2\pi f_h t)^x \quad (8)$$

theoretical raw current waveform calculated from eq 8 is shown in Figure 2A for  $f_e = 16$  Hz and  $f_h = 80$  Hz and amounts to a product of the waveforms of eq 6 and 7. As will be shown experimentally, eq 8 is valid on a semiquantitative basis, provided  $f_E$  is significantly less than  $f_h$ . Matsuda (28, 29) and Compton (30) have considered ac potential perturbations on the RDE and tubular flow electrodes and have shown that the behavior of the ac current depends on the relative thicknesses of the ac diffusion layer and the hydrodynamic boundary layer. When the hydrodynamic layer of the RDE is thin relative to that which would be produced by the ac potential perturbation, the current is independent of  $f_E$  and the phase shift between  $i$  and  $f_E$  is zero. At the other extreme of high  $f_E$ , the ac diffusion layer is thin relative to the hydrodynamic layer, and the hydrodynamics have little effect on the waveform. In this high  $f_E$  limit,  $i_E$  varies with the square root of  $f_E$ . In all cases examined here, we will assume the low  $f_E$  limit, and we will demonstrate later that eq 8 is valid.

For the case where  $f_E \ll f_h$ , eq 8 describes an amplitude modulated waveform of fundamental frequency  $2f_h$ , with the amplitude modulated at a frequency  $f_E$ . It is possible to demodulate the raw current by successive synchronous detection first at  $2f_h$  and then at  $f_E$ . Alternatively, it may be noted that eq 8 is the product of two sinusoidal functions, and both the hydrodynamic and potential modulation factors may be expressed as Fourier summations of the fundamental and harmonic terms. Equations 9 and 10 contain the first three terms of the Fourier series for potential (eq 7) and hydrodynamic (eq 5) modulation, respectively. The fundamental for the hydrodynamic term equals  $2f_h$ , as noted earlier.

$$\frac{1}{1 + \theta} = A_0 + A_1 \cos 2\pi f_E + A_2 \cos 2\pi(2f_E) + \dots \quad (9)$$

$$[1 + M] \cos(2\pi f_h t)^x = B_0 + B_1 \cos 2\pi(2f_h) + B_2 \cos 2\pi(4f_h) + \dots \quad (10)$$

Equation 11 then results from substitution of the first two terms of each of the Fourier series into eq 8 and subsequent rearrangement and trigonometric substitution. Note that the resulting product contains terms for the fundamental frequencies for each modulation mode, and the sum and difference frequencies,  $2f_h \pm f_E$ . If more than the first two terms

$$\frac{i}{nFAC_{ox}^0 m_{ss}} = A_0 B_0 + A_1 B_0 \cos(2\pi f_E) + A_0 B_1 \cos 2\pi(2f_h) + \left[ \frac{A_1 B_1}{2} \right] \sin [2\pi(2f_h + f_E)] + \left[ \frac{A_1 B_1}{2} \right] \sin [2\pi(2f_h - f_E)] + \dots \quad (11)$$

are included from eq 8 and 9, then higher order terms such as  $2f_h + 2f_E$ ,  $4f_h + f_E$ , etc. would be predicted in the raw current waveform of eq 11. From an analytical standpoint, it is important to note that the capacitive and surface Faradaic background processes will not have hydrodynamically modulated components; i.e.  $B_1$  and  $B_2$  will be zero. Thus the terms at  $2f_h + f_E$  and  $2f_h - f_E$  will be zero for either charging current

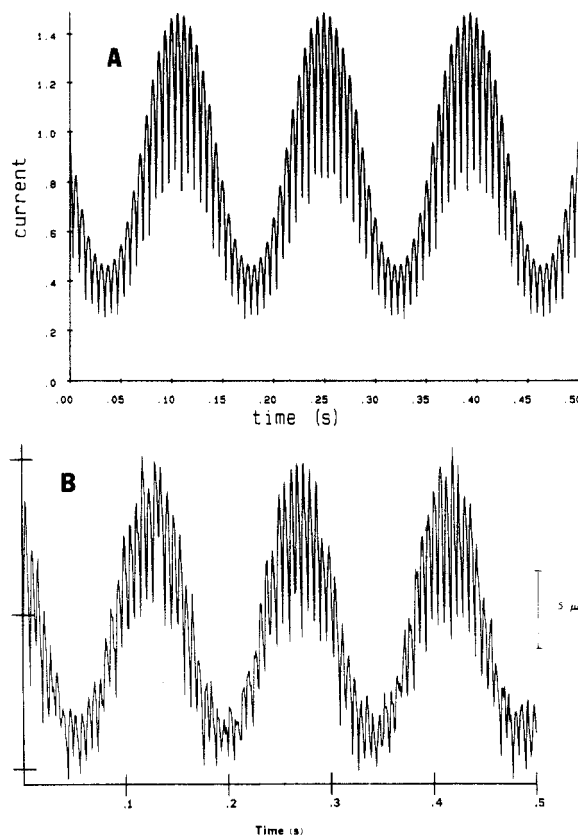


**Figure 2.** Double modulated raw current waveforms from a 25- $\mu$ m Pt electrode for 1.4 mM ferrocene in 0.1 M TBAP/acetonitrile: (A) theoretical curve from eq 8, for  $M = 0.95$ ,  $x = 0.7$ ,  $f_E = 7$  Hz,  $f_h = 80$  Hz,  $E_{oc} = E^{o'}$ ,  $\Delta E_{pp} = 60$  mV, current scale is same as figure 1A; (B) experimental, same conditions.

or surface redox processes such as oxide formation. This fact is the basis for background rejection using HMAVCV.

A Fourier transform of the diffusion limited hydrodynamic current from in Figure 1A shows components at  $2f_h$ ,  $4f_h$ ,  $6f_h$ , etc., which would be expected for a distorted sine wave. The Fourier transform of the theoretical HMAVCV current from Figure 2A is shown in Figure 3A and includes the fundamental frequencies of each individual modulation, plus the sum and difference frequencies predicted by eq 11. While a variety of combinations of the two frequencies are evident in the theoretical frequency spectrum, only the two fundamentals and the sum and difference frequencies are useful analytically, since the other components are smaller and provide no additional information.

The raw wave form may be predicted as a function of potential by varying  $E_{DC}$  in eq 8. After a Fourier transform is carried out on these raw waveforms, the dependence of each frequency component on  $E_{DC}$  may be predicted, with the results shown in Figure 4. Trace a is the magnitude of the  $2f_h$  component and has the shape of a classical hydrodynamic voltammogram since it contains no ac potential perturbation. This component results from hydrodynamic modulation at a dc potential, embodied in the third term of the right side of eq 11. Trace b is at the potential modulation fundamental and has the shape of a classical ac voltammogram. It results from the potential modulation of the dc term of the hydrodynamic waveform, given by the second term of eq 11. It is qualitatively equivalent to modulating the potential of a steady-state hydrodynamic system such as the RDE at constant rotation speed.

Trace c in Figure 5 results from either the  $2f_h + f_E$  or  $2f_h - f_E$  frequency component and should combine several features of both modulation techniques. First, the HMAVCV peak of Figure 5c has the peak-shaped appearance of an ac voltam-

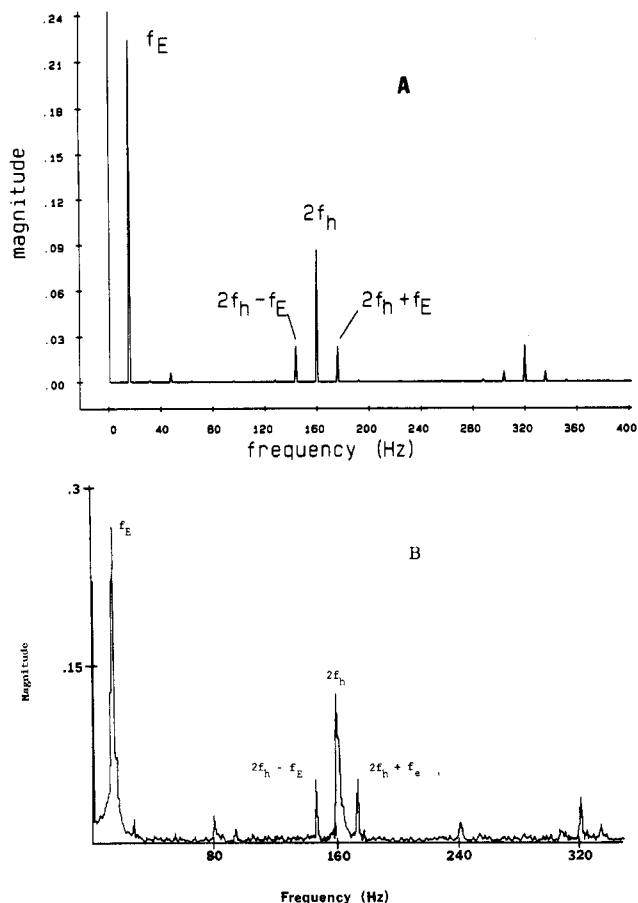


**Figure 3.** Fourier transform (magnitude spectrum) of raw current waveforms similar to those of Figure 2. Conditions are identical with those of Figure 2, except  $f_E$  was increased to 13 Hz for clarity. (A) Fourier transform of raw current calculated from eq 8. (B) Fourier transform of experimental current from Figure 2B.

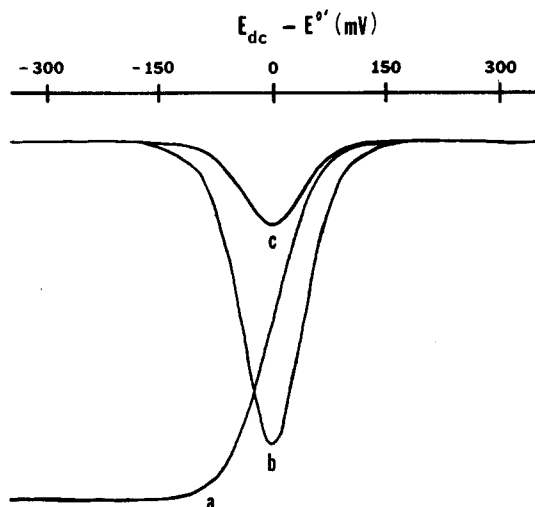


**Figure 4.** Theoretical voltammograms calculated for various frequency components. Curves are the magnitude of the appropriate Fourier component of the waveform calculated from eq 8 for a range of  $E_{dc}$ .  $f_h = 80$  Hz,  $f_E = 13$  Hz. Curve a,  $2f_h$  component; (b),  $f_E$ ; (c)  $2f_h + f_E$ .

mogram rather than the sigmoidal shape of a conventional hydrodynamic voltammogram, improving resolution and background correction. As it is a differential rather than absolute measurement, it should be less sensitive to processes that vary slowly with potential. Second, since the hydrodynamically modulated current results only from freely diffusing material, the HMA CV peak should have a greatly reduced background from capacitance and surface Faradaic processes.

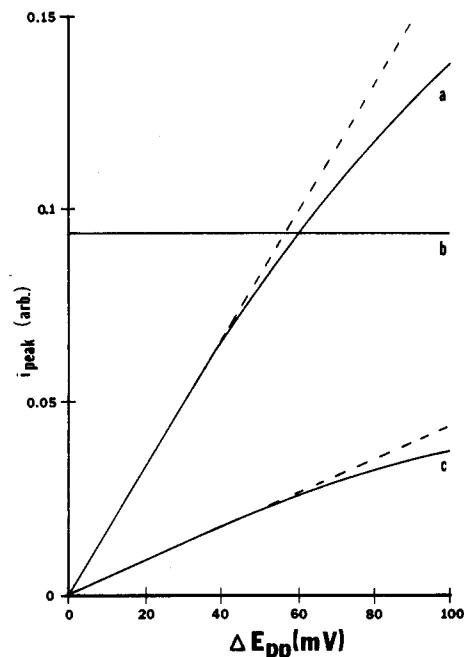


**Figure 5.** Effect of  $\Delta E_{pp}$  on peak currents for calculated HMA CV voltammograms at three frequencies, determined from results similar to those in Figure 4.  $f_E = 13$  Hz,  $f_h = 80$  Hz,  $E_{dc} = E^0$ . Dashed lines are extensions of linear portions of curves a and c. Solid lines: (a)  $f_E$ ; (b)  $2f_h$ ; (c)  $2f_h + f_E$ .

For background currents that are not mass transport controlled, the second and higher terms on the right side of eq 10, and therefore  $B_1, B_2, \dots$ , will be zero and the  $2f_h \pm f_E$  components will be negligible. Thus one should be able to observe ac voltammograms with a great reduction of background signal, a feature of clear importance when using solid electrodes.

HMA CV voltammograms similar to that in Figure 4c calculated for different values of  $\Delta E$  show a slight increase in peak width as the potential modulation amplitude is increased. As with other potential modulation techniques such as ac voltammetry and differential pulse polarography, the peak width is a weak function of  $\Delta E$  when  $\Delta E$  is less than 50 mV. Figure 5 shows several theoretical plots of the demodulated currents as functions of  $\Delta E$ . As expected, the purely hydrodynamic current is independent of  $\Delta E$ , since it is a function of only  $E_{dc}$  and potential independent variables. The magnitude of the ac currents at  $f_E$  or  $2f_h + f_E$  increases linearly at small  $\Delta E$  and then exhibits negative curvature when  $\Delta E$  is greater than approximately 50 mV.

## EXPERIMENTAL SECTION

The cell and electrodes were the same as those reported previously (18), with the working electrode consisting of a 1 cm long, 25  $\mu\text{m}$  diameter Pt wire (Goodfellow Metals, Cambridge, England) sealed in glass, with 3 mm of the wire exposed to the solution. The diameter of the glass at the point where the wire emerged into the solution was about 3 mm, but this value appeared to have little effect on the observed current. The wire was vibrated sinusoidally in a direction perpendicular to the wire axis as described previously (18), with a peak to peak vibration amplitude of 0.81 mm. The voice coil vibration exciter (PM type 4810, Bruel and Kjaer Instruments, Marlborough, MA) was driven by a 50-W Kepco power amplifier which was in turn driven by a function generator, as described below. A vibration frequency of 80 Hz was chosen for all experiments, as a value higher than a mechanical resonance at 50 Hz yet lower than a decrease in the response which begins above 80 Hz. As noted previously, the hydrodynamically modulated signal improves for smaller electrodes, but wires with diameters smaller than 25  $\mu\text{m}$  are insufficiently strong. Thus 25  $\mu\text{m}$  was the diameter used for all experiments reported here. The electrode was cleaned occasionally in concentrated  $\text{H}_2\text{SO}_4$  followed

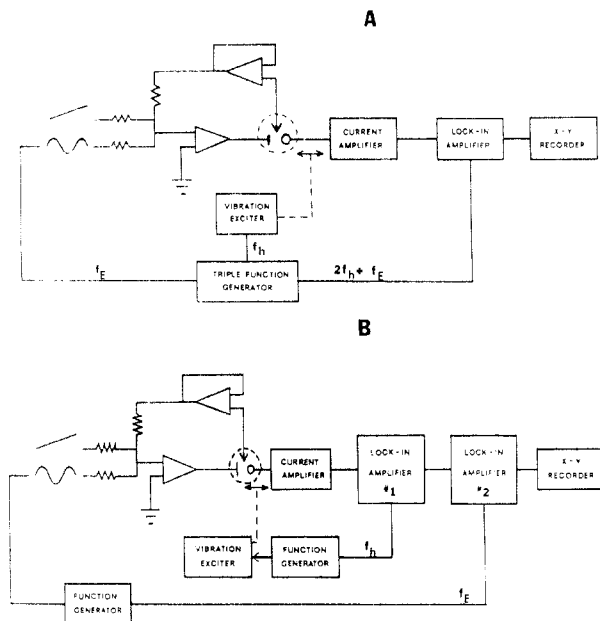


**Figure 6.** Experimental apparatus for (A) intermodulation detection of HMAVCV in which the LIA demodulates the current component at  $2f_h + f_E$ . (B) Sequentially demodulated HMAVCV (SHMAVCV), in which successive LIA's demodulate first the hydrodynamic component at  $2f_h$  and then the potential modulation at  $f_E$ . See text and ref 32 for further details.

by thorough rinsing in Nanopure water (Sybron Barnstead, Danvers, MA).

Ferrocene was obtained from Strem Chemicals (Danvers, MA) and was purified by sublimation according to a published procedure (31). Tetrabutylammonium perchlorate (Southwestern Analytical) and high-purity UV grade acetonitrile (Burdick and Jackson) were used as received. 1,1'-Bis(hydroxymethyl)ferrocene (BHMF) was a gift from Professor T. Kuwana of the University of Kansas.

A conventional three-electrode potentiostat was used to operate the cell, with the working electrode at virtual ground. The current was monitored with a Keithley Model 427 current amplifier with a gain of  $10^4$ – $10^7$  V/A. The applied potential was the sum of a dc level, a linear ramp, and a sinusoidal ac potential modulation, in the 1–30 Hz frequency range. Thus experiments could be conducted at fixed dc potential with or without an ac modulation or in scanning mode with a superimposed ac perturbation.

With an ac potential modulation present at frequency  $f_E$  and an electrode vibrated at a frequency  $f_h$ , the current from this double modulated experiment may be monitored in several ways. In some cases the raw current was recorded with a Tektronix 7854 digital oscilloscope and plotted after transfer of the waveform to an Apple computer. The principal experiments involved demodulation of the complex HMAVCV current waveform by one of the following two methods. The HMAVCV intermodulation approach involved monitoring a sideband of the hydrodynamically modulated current at a frequency of  $2f_h + f_E$ . A block diagram of this arrangement is shown in Figure 6A. The key component is a triple function generator built by the OSU Chemical Instrumentation support group, which provides three waveforms with fixed phase relationship. A master clock is monitored by three arithmetic circuits which produce square waves at  $f_E$ ,  $f_h$ , and  $(2f_h + f_E)$  with periods that are integer multiples of the master clock period. The  $f_E$  and  $f_h$  square waves are converted to sinusoids which drive the potentiostat and vibrator, respectively, and the square wave at  $2f_h + f_E$  is provided as the reference for a PARC 186A lock-in amplifier (LIA). Since all three waveforms are phase locked relative to the same master oscillator, their phase relationships remain constant throughout an experiment. The schematic for the triple function generator is presented elsewhere (32). The output of the LIA is proportional to the ac current component with a frequency of  $2f_h + f_E$ , and was monitored with an x-y recorder whose x axis was driven with the potential ramp. HMAVCV voltammograms thus consisted of plots of the ac current

synchronously demodulated at  $2f_h + f_E$  as a function of potential.

The second mode of current demodulation will be referred to as sequential and involved successive LIA's operating first at  $2f_h$ , then at  $f_E$ , as shown in Figure 6B. An 80-Hz sinusoid driving the vibration exciter was used as a reference to LIA1 (PARC 186A) which was operated in  $2f$  mode. Its output was proportional to the  $2f_h$  component of the raw current. Provided the time constant of LIA1 was much less than the period of the potential modulation, the output of LIA was a slightly distorted sine wave with frequency  $f_E$ , but demodulated with respect to hydrodynamics. LIA2 was then used to demodulate this waveform, producing a signal proportional to the effect of the potential modulation on the hydrodynamically modulated current.

## RESULTS

The observed raw hydrodynamically modulated current obtained at the diffusion limit for the oxidation of ferrocene is shown in Figure 1B. The observed and theoretical curves agree, indicating that eq 6 is a reasonably accurate expression for the shape of the hydrodynamic waveform. Fourier transforms of both the experimental and theoretical curves for the diffusion limited case demonstrate the presence of a dominant modulated component at  $2f_h$ , with harmonics at  $4f_h$ ,  $6f_h$ , etc., as well as a small contribution at  $f_h$  due to vibration asymmetry.

An experimental raw current waveform for the HMAVCV experiment represented by eq 8 is shown in Figure 2B. Several qualitative features of this complex waveform deserve note, all of which are predicted from eq 8 and 11. First, the dominant low-frequency component at frequency  $f_E$  results from potential modulation of the hydrodynamic steady-state current, i.e. the second term on the right side of eq 11. Second, the hydrodynamic "fundamental" at  $2f_h$  is prominent, as predicted by the third term in eq 11. Third, the envelope of the hydrodynamic modulation is itself modulated at  $f_E$ , with a large magnitude on the peaks of the  $f_E$  waveform and smaller magnitude on the valleys. The amplitude modulation of the  $2f_h$  hydrodynamic "carrier" results in the fourth and fifth terms of eq 11. It may also be expressed as the term from which the fourth and fifth terms of eq 11 were derived, i.e.  $A_1B_1(\cos 2\pi f_E) \cos 2\pi(2f_h)$ . The latter expression describes an amplitude modulated waveform with carrier frequency  $2f_h$  and modulation frequency  $f_E$  and can be restated as sum and difference frequencies as in eq 11.

Figure 3B shows the Fourier transform of the experimental raw current waveform of Figure 2B, and demonstrates the presence of components at  $2f_h$ ,  $f_E$ , and  $2f_h \pm f_E$ . By use of the appropriate reference waveform, it was possible to monitor each component of the HMAVCV raw current while scanning the potential. For the case of the  $2f_h + f_E$  component, the triple function generator provided the necessary reference waveform. The experimental voltammograms are shown in Figure 7 for demodulation frequencies equal to  $f_E$ ,  $2f_h$ , and  $2f_h + f_E$ . The demodulated currents are proportional to the amplitudes of the Fourier components at the various frequencies and qualitatively agree with the theoretical plots of Figure 4. The sigmoidal response at  $2f_h$  is the same as a diffusion limited hydrodynamic modulation experiment (Figure 1) with no effect from the potential modulation. This response results from the third term of eq 11. The curve obtained at  $f_E$  is analogous to the classical ac voltammetric response (27), with mass transport at steady state (second term of eq 11). The response at  $2f_h + f_E$  is the double-modulated waveform which arises from the fourth term on the right side of eq 11. While smaller in absolute magnitude, it has the same shape as the simple ac voltammetric response at  $f_E$ , with the peak width shown in Table I. The larger than ideal peak width at low  $\Delta E$  was determined by the LIA response characteristics during scanning rather than the reversibility of the redox system.

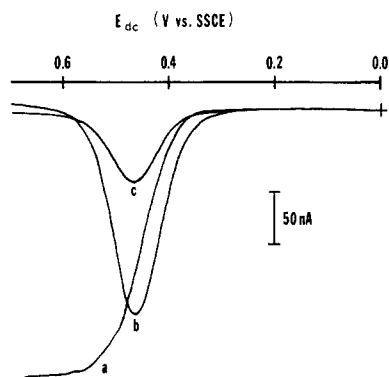


**Figure 7.** Experimental voltammograms obtained by demodulation of the HMAVCV waveform at various frequencies. For all cases,  $f_E = 13$  Hz,  $f_h = 80$  Hz,  $\Delta E_{pp} = 50$  mV, 25- $\mu$ m Pt electrode in  $7 \times 10^{-5}$  M ferrocene in 0.1 M TBAP/acetonitrile, scan rate 10 mV/s. Curve a,  $2f_h$  component recorded with vibrator drive providing LIA reference and LIA operating in  $2f$  mode ( $90^\circ$  phase shift); b, demodulated at  $f_E$ , with ac potential as LIA reference ( $45^\circ$  phase shift); c, demodulated at  $2f_h + f_E$  with triple function generator providing a reference to the LIA ( $105^\circ$  phase shift). LIA time constant was 0.3 s in all cases. Note that conditions match those of the theoretical plots of Figure 4.

**Table I. Experimental Peak Widths at Half Maximum for Intermodulation HMAVCV<sup>a</sup>**

$\Delta E_{pp}$ , mV	peak width (HMAVCV), mV
20	102.5
40	102.5
60	105.0
80	115.0
100	122.5

<sup>a</sup> Ferrocene in 0.1 M TBAP/acetonitrile on a Pt microwire.

The  $f_E$  and  $2f_h$  curves in Figure 7 were easily recorded by use of a single LIA with either the potential modulation waveform serving as a reference (for  $f_E$ ) or by monitoring the second harmonic of the waveform driving the vibrator. The  $2f_h + f_E$  component was significantly more difficult to record, since the reference waveform must be synthesized from  $f_E$  and  $f_h$  with suitable and constant phase. An experimental consequence of using the  $2f_h + f_E$  frequency is very important to the practical utility of HMAVCV. At millimolar levels of ferrocene in acetonitrile, the HMAVCV response has the predicted peak shape already demonstrated in Figure 4, with a slight, low-frequency ( $\sim 1$  Hz) oscillation apparent at and near the peak potential. At lower concentration, the oscillation is more pronounced and seriously interferes with analytical measurements. Its frequency and magnitude depended strongly on the choice of  $f_E$  and  $f_h$  and on the proximity of  $E_{dc}$  to  $E^{\circ'}$ , and its frequency was higher on the positive side of  $E^{\circ'}$  than on the negative side. The most likely source of the oscillation is a beat frequency between the  $2f_h + f_E$  component and other frequencies present in the raw waveform, e.g.  $2f_h$ . Whatever its origin, the oscillatory interference adversely affected detection limits to the point where analytical utility was compromised.

The interfering oscillation occurring when monitoring the  $2f_h + f_E$  component may be avoided by sequential demodulation of the  $2f_h$  component. Voltammograms using the apparatus of Figure 6B are shown in Figure 8. While similar in appearance to the  $2f_h + f_E$  case of Figure 4 (curve C), the voltammograms obtained with sequential demodulation did not exhibit the interfering oscillations. The peak response was linear from  $4.3 \times 10^{-7}$  to  $6.5 \times 10^{-4}$  M, with a slope of  $7.1 \times 10^{-5}$  A/M. The correlation coefficient of the log (current) vs. log (concentration) plot was 0.9973 over 3 decades. As shown in Figure 6, the sequentially demodulated HMAVCV

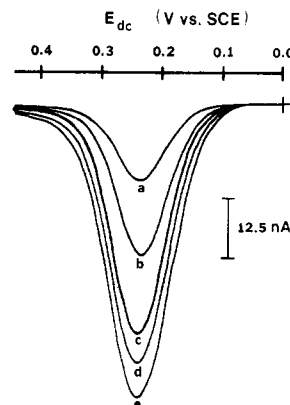


**Figure 8.** Effect of  $\Delta E_{pp}$  on experimental SHMACV response.  $F_h = 80$  Hz,  $F_E = 3$  Hz, 0.6 mM BHMF in pH 7 phosphate buffer, 25- $\mu$ m Pt microcylinder, 1 mV/s scan rate. Curves a–e are for  $\Delta E_{pp} = 20, 40, 60, 80,$  and 100 mV, respectively.

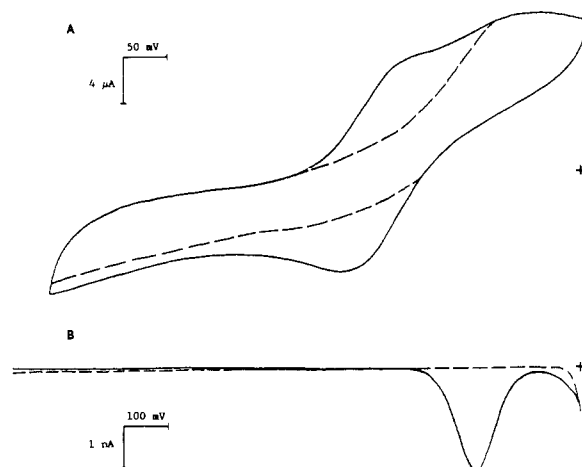


**Figure 9.** Comparison of a cyclic voltammogram using a conventionally sized Pt disk electrode with double modulation voltammograms using a Pt microcylinder electrode. Solid lines were obtained from BHMF in pH 7 citric acid/phosphate buffer, while the dashed lines are of the blank buffer solution. (A) Conventional cyclic voltammogram from a 1.5 mm diameter Pt disk electrode; [BHMF] =  $6.5 \times 10^{-4}$  M. (B) SHMACV from a 25  $\mu$ m diameter Pt microcylinder electrode; [BHMF] =  $6.5 \times 10^{-5}$  M,  $f_h = 80$  Hz,  $f_E = 3$  Hz,  $\Delta E_{pp} = 60$  mV. Note the difference in potential and current scales between the two voltammograms.

(SHMACV) response depends on  $\Delta E_{pp}$  in a fashion similar to conventional ac voltammetry (27) and our previously reported square wave technique (33).

Since  $B_1, B_2, \dots$  in eq 3 are zero for any process which is not mass transport controlled, the intermodulation or the sequentially demodulated response should have negligible contributions from surface Faradaic and capacitive background currents. As predicted theoretically, the SHMACV response should reject background at least as well as hydrodynamic modulation voltammetry. Figure 9A shows a conventional cyclic voltammogram of BHMF in pH 7 citrate/phosphate buffer with a conventional 1.5 mm diameter Pt disk electrode. At a relatively high concentration of 0.65 mM, the BHMF is obscured by background current, making determinations at lower concentrations difficult. At a factor of 10 lower concentration of BHMF, the SHMACV response shows much lower background and greatly extended anodic potential range, due to suppressed contribution from surface Faradaic reactions (Figure 9B). The positive potential limit was determined by overload of the detection electronics caused by the large dc current present, but the response was flat to +1.3 V vs. SCE in pH 7 buffer.

Voltammograms for the SHMACV technique at low concentrations are shown in Figure 10 for BHMF in aqueous

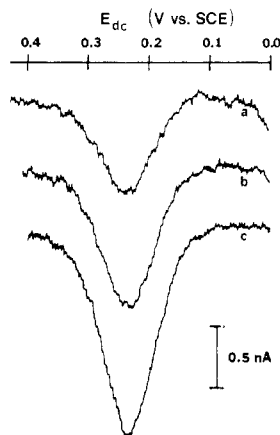


**Figure 10.** SHMACV for BHMf in pH 7 phosphate buffer, near the detection limit:  $f_h = 80$  Hz;  $f_E = 3$  Hz; 1 mV/s scan rate;  $\Delta E = 60$  mV; (a) 1.7  $\mu\text{m}$ , (b) 2.6  $\mu\text{m}$ , (c) 3.9  $\mu\text{m}$ .

**Table II. Detection Limits (mol/L) for Several Modulation Techniques at a Platinum Electrode<sup>a</sup>**

square wave voltammetry (33)	$8 \times 10^{-6}$
hydrodynamic modulation voltammetry (18)	$9 \times 10^{-7}$
intermodulation HMA CV	$1 \times 10^{-6}$
SHMACV	$4 \times 10^{-7}$

<sup>a</sup> BHMf in water at pH 7, platinum working electrode.

solution. The detection limit, defined as a signal of twice the root mean square noise of a blank is  $4 \times 10^{-7}$  M. This value is compared to several modulation techniques for solid electrodes in Table II.

For the range of  $f_E$  from 3 to 130 Hz, the SHMACV response increased by less than 33%, indicating a weak dependence on  $f_E$ . If the SHMACV response had a  $f_E^{1/2}$  dependence, as expected for  $f_E \gg f_h$ , the increase over this frequency range should have been 660%. This observation validates the assumption that the hydrodynamic boundary layer is thin relative to that which would be caused by a potential perturbation at a frequency of  $f_E$ . By use of the approach of Pratt (34), the hydrodynamic boundary layer has a thickness of ca. 3  $\mu\text{m}$ , whereas the potential modulation boundary layer would be on the order of 20  $\mu\text{m}$ , based on the value of  $(Dt)^{1/2}$  for one cycle of a 3-Hz potential modulation. The peak phase for the SHMACV signal occurred at  $210^\circ$  for the  $2f_h$  lock-in and  $-15^\circ$  for the  $f_E$  lock-in. The observed magnitudes of either the SHMACV or intermodulation peaks increased linearly with  $\Delta E$  up to about 50 mV, then exhibited a negative deviation from linearity, as predicted theoretically.

## DISCUSSION

There are two major factors which affect the analytical utility of the HMA CV approach: the nature of the raw modulated current and the method by which it is demodulated to produce a useful response. The key feature of the raw current is the fact that only mass transport controlled reversible or quasi-reversible redox systems will be modulated at both  $f_E$  and  $2f_h$ . Stated mathematically,  $B_1$  at eq 11 will be zero for any process which is unaffected by mass transport, e.g. capacitance and surface Faradaic reactions. Thus the third and fourth terms of eq 11, corresponding to monitoring the  $2f_h$  or  $2f_h + f_E$  components, are zero for surface Faradaic and capacitive processes. If only the hydrodynamic modulation is considered, this feature is basically the same as that employed in other hydrodynamic modulation methods, with one significant exception. The microwire electrode permits the use of higher modulation frequencies, reducing flicker noise

and upshifting the frequency into a range more suitable for detection by a LIA (e.g. 160 Hz vs 0.1–15 Hz for a modulated RDE). Before the potential modulation is considered, the net result of using a microwire electrode is higher performance than other HMV techniques with respect to modulation frequency, at the cost of more complex hydrodynamics which can only be described in less rigorous terms than an RDE or flow cell.

The imposition of a potential modulation on top of an already hydrodynamically modulated current is equivalent mathematically to setting  $A_1$  in eq 11 to a nonzero value. The second term of eq 11 will produce the large fundamental oscillation at  $f_E$ , but this term will not discriminate against background current because both  $A_1$  and  $B_0$  may be nonzero for surface or capacitive processes. For example, formation of a platinum oxide species will be potential dependent ( $A_1 \neq 0$ ) and will have a nonzero value for a stationary electrode ( $B_0 \neq 0$ ). Thus the current at  $f_E$  will include contributions from the major background processes common to solid electrodes and the detection limits of conventional ac voltammetry will be dictated by the presence of these currents. The fourth and fifth terms of eq 11 incorporate double modulation and retain the background rejection of single (hydrodynamic) modulation. Since  $B_1$  is zero for non-mass-transport-controlled processes, currents measured at  $2f_h \pm f_E$  will be zero for background processes. In addition, only potential-modulated processes, which therefore have a nonzero  $A_1$ , will contribute to the fourth or fifth terms. The result is the requirement that a process be both mass transport controlled and potential modulated to contribute to the current at  $2f_h \pm f_E$ . The Fourier transform of the raw current shown in Figure 3B verifies that such frequency components exist for ferrocene in acetonitrile.

Once the existence of the HMA CV component in the raw waveform is established, there remains the technical issue of monitoring its particular frequency, whose magnitude may be small, in the presence of substantially larger components such as the  $f_E$  fundamental. The conceptually simple approach of monitoring single frequencies with a LIA produced Figure 7c, but it is not the optimum approach for detecting the  $2f_h + f_E$  component because of apparent interferences from nearby modulation components. The result of this interference was distorted voltammograms and relatively poor detection limits. The mathematically equivalent SHMACV approach is free from the interference observed on the  $2f_h + f_E$  component and leads to better detection limits. The two methods have comparably good linearity with concentration and share the background rejection resulting from hydrodynamic modulation.

The dependence of SHMACV response on the  $\Delta E_{pp}$  is qualitatively similar to that predicted theoretically and also to analogous plots for ac voltammetry and a square wave technique employing a microwire electrode (33). Since the waveform after demodulation of the  $2f_h$  carrier is analogous to an ac voltammogram conducted at a hydrodynamic steady state, it should have the  $\Delta E$  dependence of a normal ac wave. The SHMACV experiment amounts to ac voltammetry with the added feature of background rejection through hydrodynamic modulation.

While HMA CV techniques do permit sensitive voltammetry on solid electrodes in aqueous solution, there is a price in speed and electrode life.  $f_E$  must be much less than  $2f_h$ , both to validate the assumptions of the theory and to permit successive demodulation by two LIA's. A low  $f_E$  requires a fairly long LIA time constant ( $\sim 1$ –3 s), forcing low scan rates, compared to rapid scan pulse techniques such as square wave voltammetry (35, 36). The net result is a scan time comparable to differential and normal pulse polarography. In addition,

the double modulation scheme drives the Faradaic process fairly hard, with the possibility of electrode fouling. The current densities will typically be comparable to microdisk electrodes rather than the usual millimeter scale solid electrodes.

The advantages of double modulation voltammetry are several and will be particularly important when background current is severe. First, Figure 9 demonstrates outstanding rejection of background current compared to conventional voltammetry. Compared to HMV, the SHMACV technique has the advantage of a peak rather than wave response, leading to improved detection limits and resolution. As has been amply demonstrated with differential pulse and square wave voltammetry compared to dc polarography, the peak response resulting from the differential nature of these methods is more analytically useful. Finally, the rejection of background extends the potential range of the electrode/electrolyte combination farther into the solvent breakdown region, permitting significant (0.2–0.3 V) extension of the useful potential range accessible to solid electrodes.

#### ACKNOWLEDGMENT

The authors thank Dale Karweik, director of the Chemical Instrumentation support group, for fabrication of the triple function generator and for discussions on signal processing.

Registry No. BHMf, 62524-59-8; ferrocene, 102-54-5.

#### LITERATURE CITED

- (1) Wang, J. *Talanta* **1981**, *28*, 369–376.
- (2) Miller, B.; Bruckenstein, S. *J. Electrochem. Soc.* **1974**, *121*, 1558–1562.
- (3) Miller, B.; Bruckenstein, S. *Anal. Chem.* **1974**, *46*, 2026–2033.
- (4) Tokuda, K.; Bruckenstein, S.; Miller, B. *J. Electrochem. Soc.* **1975**, *122*, 1316–1322.
- (5) Tokuda, K.; Bruckenstein, S.; Miller, B. *J. Electrochem. Soc.* **1979**, *126*, 431–436.
- (6) Kanzaki, Y.; Bruckenstein, S. *J. Electrochem. Soc.* **1979**, *126*, 437–441.

- (7) Blaedel, W. J.; Engstrom, R. C. *Anal. Chem.* **1978**, *50*, 476–479.
- (8) Blaedel, W. J.; Boyer, S. L. *Anal. Chem.* **1971**, *43*, 1538–1540.
- (9) Blaedel, W. J.; Iverson, D. G. *Anal. Chem.* **1977**, *49*, 1563–1566.
- (10) Blaedel, W. J.; Wang, J. *Anal. Chem.* **1979**, *51*, 799–802.
- (11) Blaedel, W. J.; Yim, Z. *Anal. Chem.* **1980**, *52*, 564–566.
- (12) Blaedel, W. J.; Wang, J. *Anal. Chim. Acta* **1980**, *116*, 315–322.
- (13) Blaedel, W. J.; Wang, J. *Anal. Chem.* **1980**, *52*, 1697–1700.
- (14) Wang, J.; Dewald, H. D. *Anal. Chim. Acta* **1982**, *136*, 77–84.
- (15) Wang, J.; Freiha, B. A. *Analyst (London)* **1983**, *108*, 685–690.
- (16) Pratt, K. W., Jr. Ph.D. Thesis, Iowa State University, 1981.
- (17) Pratt, K. W., Jr.; Johnson, D. C. *Electrochim. Acta* **1982**, *27*, 1013–1021.
- (18) Schuette, S. A.; McCreery, R. L. *Anal. Chem.* **1986**, *58*, 1778–1782.
- (19) Bard, A. J.; Faulkner, L. R. *Electrochemical Methods*; Wiley: New York, 1980; p 28.
- (20) Lindsey, A. J. *J. Phys. Chem.* **1952**, *56*, 439–442.
- (21) Harris, E. D.; Lindsey, A. J. *Analyst (London)* **1951**, *76*, 647–649.
- (22) Moorhead, E. D.; Bhat, G. A.; Stephens, M. M. *J. Chem. Technol. Biotechnol.* **1981**, *31*, 259–272.
- (23) Moorhead, E. D.; Stephens, M. M.; Bhat, G. A. *Anal. Lett.* **1981**, *14*(A4), 219–240.
- (24) Weber, S. G. *J. Electroanal. Chem.* **1983**, *145*, 1–7.
- (25) Hanekamp, H. B.; deJong, H. G. *Anal. Chim. Acta* **1982**, *135*, 351–354.
- (26) Hanekamp, H. B.; Van Nieuwerkerk, H. J. *Anal. Chim. Acta* **1980**, *121*, 13–22.
- (27) Smith, D. E. In *Electroanalytical Chemistry*; Bard, A. J., Ed.; Marcel Dekker: New York, 1966; Vol. 1, Chapter 1.
- (28) Tokuda, K.; Matsuda, H. *J. Electroanal. Chem.* **1977**, *82*, 157–171.
- (29) Tokuda, K.; Matsuda, H. *J. Electroanal. Chem.* **1978**, *90*, 149–163.
- (30) Compton, R. G.; Sealy, G. R. *J. Electroanal. Chem.* **1983**, *145*, 35–41.
- (31) Jolly, W. J. *The Synthesis and Characterization of Inorganic Compounds*; Prentice Hall: Englewood Cliffs, NJ, 1970, p 486.
- (32) Schuette, S. A. Ph.D. Thesis, The Ohio State University, 1987.
- (33) Schuette, S. A.; McCreery, R. L. *J. Electroanal. Chem.* **1985**, *191*, 329–342.
- (34) Pratt, K. W. *Anal. Chem.* **1984**, *56*, 1967–1970.
- (35) O'Dea, J. J.; Osteryoung, J.; Osteryoung, R. A. *Anal. Chem.* **1981**, *53*, 695–701.
- (36) O'Dea, J. J.; Osteryoung, J.; Osteryoung, R. A. *J. Phys. Chem.* **1983**, *87*, 3911–3918.

RECEIVED for review March 2, 1987. Accepted July 3, 1987. The work was supported by the Chemical Analysis Division of the National Science Foundation.

## Liquid Chromatography–Photolysis–Electrochemical Detection for Organoiodides. 1. Optimization and Application

Carl M. Selavka and Ira S. Krull\*

Barnett Institute of Chemical Analysis and Department of Chemistry, Northeastern University, Boston, Massachusetts 02115

**An improved high-performance liquid chromatographic detection method has been applied for the trace determination of iodinated organic compounds. The method, which incorporates postcolumn, on-line UV irradiation prior to oxidative electrochemical (EC) detection, exploits the facile photochemical dissociation of the C–I bond to form anionic iodide and a number of solvolyzed products. Following bond cleavage, iodide is readily detected amperometrically at moderate oxidative potentials, allowing for the determination of a number of organoiodides at the 25–75 pg level. Following optimization of experimental parameters, the detection approach is linear over 3 orders of magnitude, and enhanced selectivity is demonstrated through the utilization of chromatographic retention times, dual electrode response ratios, and qualitative lamp on/off responses for analyte identification. The method is validated in a single-blind study and is successfully applied to the determination of liothyronine (T<sub>3</sub>) in tablets.**

Halogenated organic compounds are widely employed as solvents, reagents in organic syntheses, additives in manufactured products, agricultural fumigants, flame retardants, and pharmaceuticals (1, 2). Unfortunately, many of these compounds are toxic, mutagenic, or carcinogenic. Typically, gas chromatographic (GC) methods are employed for the determination of organohalogenes, due to the volatile nature of most of these compounds, with selective and sensitive detection obtained by using the electron capture detector (ECD) or mass spectrometry. Additionally, halogen-selective detection in GC may be obtained using near-infrared emission in an inductively coupled plasma (3) or a microwave induced plasma (4).

There is a need for alternative methods of analysis for those organohalogenes which are insufficiently volatile for routine GC–ECD analysis, or for laboratories which require an analytical method to confirm GC determinations (5). In addition, time-consuming sample cleanup may be necessary prior to GC